Biophysical Chemistry 180–181 (2013) 44–54

Contents lists available at ScienceDirect

Biophysical Chemistry

journal homepage: http://www.elsevier.com/locate/biophyschem

# New gluconamide-type cationic surfactants: Interactions with DNA and lipid membranes

Paweł Misiak [a,*], Kazimiera A. Wilk [b,1], Teresa Kral [a,c,2], Edyta Woźniak [a,2], Hanna Pruchnik [a,2], Renata Frąckowiak [b,1], Martin Hof [c], Bożenna Różycka-Roszak [a,2]

[a] Department of Physics and Biophysics, Wrocław University of Environmental and Life Sciences, ul. Norwida 25, 50-375 Wrocław, Poland
[b] Organic and Pharmaceutical Technology Group, Faculty of Chemistry, Wrocław University of Technology, Wybrzeże Wyspiańskiego 27, 50-370 Wrocław, Poland
[c] J. Heyrovsky Institute of Physical Chemistry of the ASCR, v.v.i., Dolejškova 2155/3, 182 23 Prague 8, Czech Republic

## HIGHLIGHTS

- New cationic glucose-derived CnGAB surfactants are synthesized using green chemistry.
- Compaction of DNA with CnGAB is studied by fluorescence correlation spectroscopy.
- Interactions of CnGABs with DPPC liposomes are studied by DSC and spectroscopy.
- Theoretical modeling of interaction properties of the surfactants is presented.
- $C_{16}$GAB is a promising candidate as a component of gene-delivery carrier systems.

## GRAPHICAL ABSTRACT

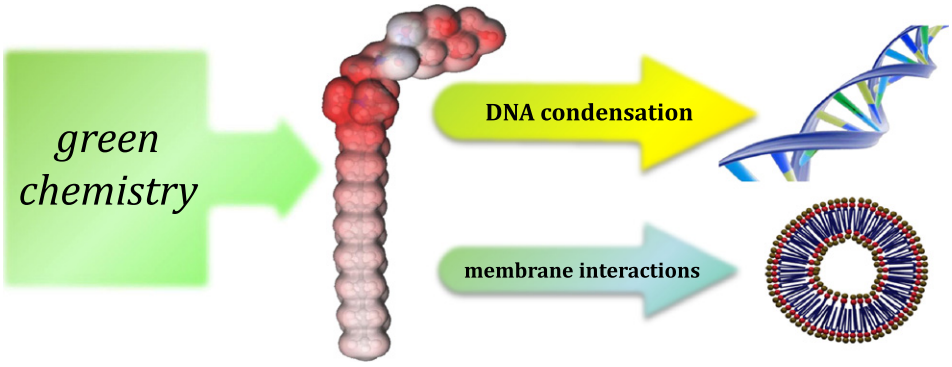


## ARTICLE INFO

*Article history:*
Received 29 March 2013
Received in revised form 4 June 2013
Accepted 8 June 2013
Available online 21 June 2013

*Keywords:*
Glucose-derived surfactant
Soft surfactant
Cationic surfactant
DNA compaction
Lipid bilayer
Molecular modeling

## ABSTRACT

New linear cationic surfactants – 2-(alkyldimethylammonio)ethylgluconamide bromides, denoted as $C_n$GAB, $n = 10, 12, 14$ and 16 – were synthesized from natural resources and characterized with respect to their potential as gene-delivery agents in gene therapy applications. Interactions with plasmid DNA and with model membranes were studied both experimentally and theoretically. The compounds with $n = 12, 14$ and 16 show exponentially increasing ability to fully condense DNA. $C_{16}$GAB condenses DNA at 1:1 surfactant to nucleotide molar ratio. Furthermore, $C_n$GABs interact with model membrane, slightly lowering the temperature of the main phase transition $T_m$ of the DPPC bilayer. $C_{10}$GAB is found to interact only at the membrane surface. $C_{16}$GAB reduces $T_m$ less than $C_{12}$GAB and $C_{14}$GAB, and forms domains in the bilayer at the surfactant/DPPC molar ratio of 0.1 and higher. The results suggest that $C_{16}$GAB can be a promising candidate for building gene-delivery carrier systems.



## 1. Introduction

Cationic surfactants, besides their traditional applications as antimicrobial agents, wetting agents, emulsifiers and dispersing aids, have great potential for engineering nanostructures and as important components of nanoscale drug- and gene-delivery systems [1]. In recent years, basic and applied research interest in cationic surfactants

* Corresponding author. Tel.: +48 71320 5293; fax: +48 71320 5168.
*E-mail address:* pawel.misiak@up.wroc.pl (P. Misiak).
[1] Tel.: +48 71320 2828; fax: +48 71320 3678.
[2] Tel.: +48 71320 5293; fax: +48 71320 5168.

0301-4622/$ – see front matter © 2013 Elsevier B.V. All rights reserved.
http://dx.doi.org/10.1016/j.bpc.2013.06.010

has increased, partly because of the urge to use cationic amphiphiles as vectors for gene delivery into the cell, the first step of gene therapy, a conceptually new approach for the development of delivery systems for genes.

Although frequently applied viral vectors are generally very efficient in delivering genes into targeted cells, their use is not without risk of adverse or immunogenic reactions. As a result, non-viral vectors have in many cases become the preferred means of gene delivery, although their transfection efficiency varies depending on the composition and structure of the compounds and needs to be studied and optimized. There are various limitations to the delivery of DNA, which include its stability during transit from the site of injection to the target tissue, cellular uptake by endocytosis, the endosomal/lysosomal escape of the DNA, and finally the nuclear import followed by transcription and translation of the protein of interest [2,3].

One of the important issues for the effective delivery of DNA into the cell is using it in the compacted form, which protects it from attack by nucleases. The compaction of DNA together with the reduction of the negative charges of its backbone is believed to facilitate the uptake of nucleic acids through the cellular membrane [4,5]. Since the strong binding of cationic surfactants to DNA allows these two effects to be fulfilled, it is not surprising that the complexation with cationic lipids is considered as an important factor of the strategy for the delivery of DNA to cells. DNA can form complexes with positively charged nanoparticles, polyelectrolytes and amphiphilic structures [6]. Various synthetic systems of cationic character, including nanoparticles [7], liposomes [8], synthetic lipid/surfactants [9], polymers and dendrimers [10], have been reported to compact DNA.

The other important factor in gene transfection is related to the delivery vector, which should increase the permeability of condensed DNA through the cell membrane. In the process of endocytosis the membrane is the main barrier which has to be passed through by the drug or gene carrier without destroying it. The interactions of amphiphiles forming liposomal complexes used as non-viral vectors with a membrane should facilitate transport of DNA without destroying the membrane. Most of the synthetic cationic surfactants cannot be used for this purpose without a lipid helper, while the complexes of DNA and cationic micelles do not result in effective transfection. It is a common viewpoint to explain this low transfection efficiency by the cytotoxicity of surfactants and the low stability of these complexes upon a change in the environment [11–13]. Therefore, when introducing novel cationic amphiphiles in view of potential applications for gene delivery, it is also of primary importance to study in detail their influence on the lipid membrane.

Research in the field of cationic surfactants containing a glucose-based moiety has developed very quickly as such structures show unique properties such as mild production conditions, lower toxicity, higher biodegradability, and environmental compatibility. Recently, glucocationic surfactants of various structure – linear [14,15], dicephalic [16,17], or gemini [18,19] – have been considered to be promising candidates as gene- and drug-delivery vehicles for biomedical applications, and nowadays they are a major focus of DNA research. In view of the general developments of sugar-based surfactants and their potential applications in biomedical sciences, in the present work a series of novel cationic surfactants derived from easily accessible renewable resources is proposed. The compounds are glucose-derived 2-(alkyldimethylammonio)ethylgluconamide bromides, subsequently referred to as $C_n$GAB, with alkyl chains of length $n = 10$, 12, 14 and 16 carbon atoms (Fig. 1).

The main goal of this paper is to present the study of interactions of the newly synthesized series of soft glucose-derived surfactants with DNA and lipid membranes. Especially, their ability to compact DNA and their impact on the membrane structure and thermotropic behavior are studied in order to determine the usefulness of the surfactants in gene-delivery applications. Interactions of these new

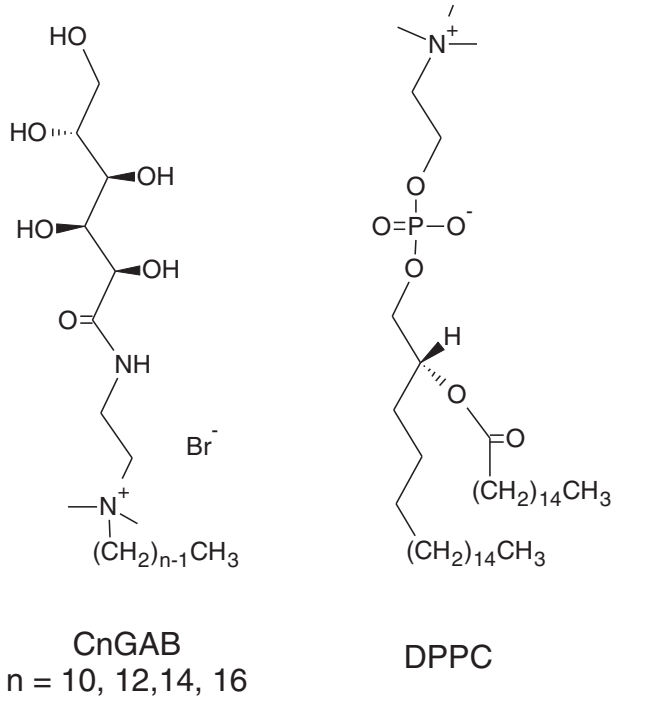


**Fig. 1.** General structure of the molecules involved in this study: 2-(alkyldimethylammonio) ethylgluconamide bromides ($C_n$GABs) and 1,2-dipalmitoyl-sn-glycero-3-phosphatidylcholine (DPPC).

cationic gluconamide bromides with DNA along with their influence on phase behavior of DPPC bilayers are interesting because of achieving a better insight into the relations between the surfactants' structure and their ability to be used in forming the DNA transfection vector. In order to understand the interaction between the studied surfactants and DNA, a single-molecule fluorescence technique, time-correlated single photon counting fluorescence correlation spectroscopy (TCSPC–FCS), was applied. The effect of the surfactants on the model lipid membrane, specifically on the lipid bilayer phase transitions, was examined by differential scanning calorimetry (DSC) and fluorescence spectroscopy using three widely used fluorescent probes. Molecular properties essential for the interactions of the surfactants with DNA and lipid molecules were studied by means of classical and quantum computational methods.

## 2. Materials and methods

### 2.1. Materials

All starting materials and solvents were of commercial grade and were not additionally purified before use. D-(+)-gluconic acid δ-lactone, *N,N*-dimethylethylenediamine, 1-bromodecane, 1-bromododecane, 1-bromotetradecane and 1-bromohexadecane were purchased from Aldrich Chemical Co. (Milwaukee, WI).

1,2-Dipalmitoyl-sn-glycero-3-phosphatidylcholine (DPPC) was purchased from Sigma Aldrich, Steinheim, Germany. Lipid purity was greater than 99%. The fluorescent probes 6-dodecanoyl-2-dimethylaminonaphthalene (Laurdan), 6-propionyl-2-dimethylaminonaphthalene (Prodan) and 1,6-diphenyl-1,3,5-hexatriene (DPH) were purchased from Molecular Probes, Eugene, Oregon USA.

### 2.2. Synthesis of surfactants: general procedure

2-(Alkyldimethylammonio)ethylgluconamide bromides ($C_n$GAB) were synthesized according to the method described in our previous paper [15]. The synthetic route for the synthesis of $C_n$GAB is

presented in Fig. 2. In the present case D-(+)-gluconic acid δ-lactone, instead of D-glucoheptono-1,4-lactone, was used in the reaction with 2-dimethylaminoethylamine to form 2-(*N*,*N*-dimethylamino) ethylgluconamide. The reaction was conducted in methanol solution at 55–60 °C for 6 h. The obtained hydrophilic semiproduct was then reacted with appropriate 1-bromoalkanes to yield the final quaternary salts 2-(alkyldimethylammonio)ethylgluconamide bromides. The quaternization reaction was performed in anhydrous ethanol by gently boiling the reaction mixture for 24 h. Semiproduct and final products were purified by recrystallization from the ethyl acetate/methanol mixture. The yields of the final products were above 70%.

Purity and chemical structures were determined by $^1$H NMR spectra (AMX-300 spectrometer; Bruker Daltonics, Germany), elemental analysis (2400 CHN analyzer; PerkinElmer, Norwalk, CT, USA) and electrospray ionization mass spectroscopy (ESI-MS) (Apex-Qe Ultra 7 T instrument; Bruker Daltonics, Germany). The ESI-MS instrument was operated in the positive ion mode and calibrated with the Tunemix™ mixture (Bruker Daltonics, Germany). The mass accuracy was better than 5 ppm. The obtained mass spectra were analyzed using the Biotools software (Bruker Daltonics, Germany).

The analysis of $^1$H NMR spectra of 2-(dodecyldimethylammonio) ethylgluconamide bromide ($C_{12}$GAB) is shown as an example: $\delta_H$ (300 MHz, DMSO-$d_6$, $Me_4Si$): 0.84 (3H, t, $J = 6.6$ Hz, $CH_3(CH_2)_9CH_2CH_2-$); 1.23 (18H, m, $CH_3(CH_2)_9CH_2CH_2-$); 1.64 (2H, m, $CH_3(CH_2)_9CH_2CH_2-$); 3.02 (6H, s, $(CH_3)_2N^+-$); 3.15 (2H, t, J = 6.0 Hz, $CH_3(CH_2)_9CH_2CH_2-$); 3.34–5.53 (signals derived from sugar residue, $HOCH_2(CHOH)_4CO-$); 8.10 (1H, t, J = 5.6 Hz, $-HNCH_2CH_2N^+-$). Elemental analysis calculated for $C_{23}H_{49}BrN_2O_7$: C, 51.26; H, 9.19; N, 5.43 found: C, 50.85; H, 9.23; N, 5.49. The ESI-MS results obtained for $C_{10}GA^+$, $C_{12}GA^+$, $C_{14}GA^+$, and $C_{16}GA^+$ cations take the values 407.31, 435.34, 463.37 and 491.41, respectively, and are equal to the calculated monoisotopic masses of the respective cations. The ESI-MS analysis also confirmed the high purity level of the compounds.

### 2.3. Time-correlated single photon counting fluorescence correlation spectroscopy (TCSPC–FCS)

To explore the surfactant–DNA interactions, a single-molecule detection technique that combines simultaneous time-correlated single-photon counting time tag mode with fluorescence correlation spectroscopy (TCSPC–FCS) was employed, as reported earlier [20–22].

Usually, the two readout parameter residence time ($\tau_{res}$) and apparent particle number (*PN*) contain information about the diffusion coefficient and the concentration of the fluorescently labeled molecules, respectively [23]. *PN* is described by the equation $PN = C \cdot V \cdot N_A$, where *C* is the molarity of the detected molecules (DNA), *V* is the confocal volume (1 fL) and $N_A$ is the Avogadro constant. The DNA concentration used in the experiments was constant at 1 nM. The theoretical *PN* to be achieved is 0.6 ± 0.2. However, in the case reported herein the multi-labeled plasmid DNA might exceed the diameter of the laser focus by about one and half times [24,25]. For the freely diffusing plasmid DNA the segmental and the Brownian motions of the whole molecule are superimposed [26], which causes an increase of the apparent number of particles in the focus and also affects the apparent residence times.

The combination of these FCS measurements with the TCSPC method allows simultaneous detection of the fluorescence lifetime. TCSPC is based on the repetitive precisely timed registration of the single photons of e.g. a fluorescence signal. The technique requires an excitation source with pulsed output of a high repetition rate. As the process of capturing a single photon is repeated several thousand or even a million times per second, a sufficiently high number of single photons is processed for the resulting fluorescence lifetime measurement. The fluorescence lifetime gives information on the local environment of the PicoGreen label. As shown earlier [24,27], it can be interpreted as a mark of DNA tight compaction.

The set-up was as follows: TCSPC–FCS measurements were performed on a MicroTime 200 inverted confocal microscope (PicoQuant, Germany) with the pulsed diode laser (LDH-P-C-470, 470 nm PicoQuant) providing 80 ps pulses at a 40 MHz repetition rate, dichroic mirror 490 DRLP and band-pass filter 515/50 (Omega Optical), and a water immersion objective (1.2 NA, 60×) (Olympus). Low power of 4 μW (at the back aperture of the objective) was chosen to minimize photobleaching and saturation. In the detection plane, a pinhole (50 μm in diameter) was used and the signal was collected by a single photon avalanche diode (SPAD, Microphoton Devices, Bolzano, Italy). Photon arrival times were stored using fast electronics (Picoharp 300, PicoQuant) in time-tagged time-resolved recording mode. Two independent times were assigned to each detected photon: (i) a time after the beginning of the measurement and (ii) a time after the previous laser pulse. The FCS data analysis was done using home-built routines (DevC++, Bloodshed Software and OriginPro70, OriginLab Corporation). The TCSPC data analysis was performed using SymPhoTime software (PicoQuant). Further details of the data evaluation are given elsewhere [23].

### 2.4. Preparation of surfactant/DNA complexes for the FCS experiments

The 10 000 bp (Bap) plasmid and PicoGreen® (PG) fluorescent dye were prepared and used as described elsewhere [22]. We used the labeling ratio 2PG/100 base pairs. After staining DNA the plasmid was titrated with various amounts of $C_n$GAB suspensions. Experiments were performed in deionized water at 25 °C.

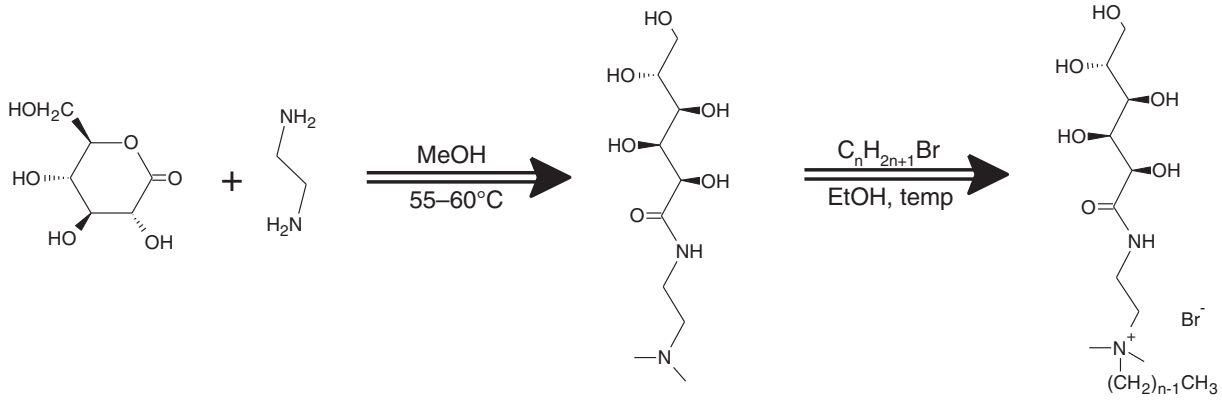


**Fig. 2.** Scheme of the synthesis route of the studied surfactants.

### 2.5. Sample preparation for DSC

Samples for DSC were prepared on multilamellar vesicles (MLVs). DPPC dissolved in chloroform was evaporated. Traces of chloroform were removed with a stream of dry hydrogen under vacuum. The lipid film was then dispersed by adding water solutions of the surfactants of appropriate concentrations. The suspension was intensively mixed at 60 °C for 15 min, loaded into a crucible and incubated at 5 °C for 5 days.

DSC studies were performed according to the protocol described earlier [28–30] using the Mettler Toledo Thermal Analysis System D.S.C. 821$^e$. The cycles were performed three times. The experimental error in temperature was ±0.2 °C.

### 2.6. Fluorescence spectroscopy of lipophilic probes Prodan, Laurdan and DPH

Small unilamellar vesicles (SUVs) of DPPC were formed. The DPPC was dissolved in chloroform and suitable fluorescent probes were added and very carefully evaporated to dryness under nitrogen. Then, the water solutions of $C_{10}$GAB, $C_{12}$GAB, $C_{14}$GAB or $C_{16}$GAB of appropriate concentrations were added. The lipid film was dispersed by agitating the flask on a vortex mixer to give a milky suspension of liposomes at a temperature above the main phase transition of DPPC. SUVs with probes were formed by sonication of lipid dispersion in water solution of surfactants. Control samples contained lipid suspension and a suitable fluorescence probe at 100:1 molar ratio.

Fluorescence intensity was measured with the Laurdan, Prodan and DPH probes. The measurements were conducted with a VARIAN CARY Eclipse fluorimeter equipped with a DBS Peltier temperature controller. The temperature of the sample was maintained with an accuracy of 0.1 °C. The excitation and emission wavelengths for the DPH probe were $\lambda_{ex} = 360$ nm and $\lambda_{em} = 425$ nm. For Laurdan and Prodan probes $\lambda_{ex} = 360$ nm while the emitted fluorescence was recorded at two wavelengths: 440 nm (gel phase) and 490 nm (liquid phase).

The generalized polarization (*GP*) for Laurdan and Prodan was calculated from the emission data using the formula [31,32]: $GP = (I_g - I_l) / (I_g + I_l)$, where $I_g$ and $I_l$ are the fluorescence intensities at the gel and the fluid phase, respectively.

The anisotropy coefficient *A* for DPH probes was calculated automatically by the apparatus' controlling software according to the standard method [33].

### 2.7. Molecular modeling

Molecular mechanics and DFT (density functional theory) calculations were done using the Materials Studio 6.0 [34] software package from Accelrys Software Inc. The semiempirical quantum calculations were done using the MOPAC2009 ver. 11.366W [35] program via the VEGA ZZ package [36].

Simulations of the conformational space of molecules and ions, similar to those used earlier [37,38], were performed within the Forcite Plus module using atomic charges fitted to the molecular electrostatic potential (ESP), obtained from the DFT calculations, and the general purpose ab-initio COMPASS force field. The simulations involved 1000 cycles of simulated annealing, each cycle consisting of 10-step heating from 300 K to 700 K and then 10-step cooling back to 300 K, with energy optimization after each cycle. The final conformations with energies within the range of $k_BT$ ($k_B$ — Boltzmann constant, $T$ — temperature, equal to 300 K) from the lowest value up were then optimized using the DFT method. Then the conformation of the lowest final energy was chosen as the most probable one for further considerations, e.g. for calculating molecular electrostatic potential surfaces.

The DFT computations were performed using the DMol$^3$ module [39] with the double-numerical basis set with polarization functions (DNP) version 4.4 [40] and the gradient-corrected functional VWN-BP [41–43]. For the molecules with optimized geometry, molecular properties such as electronic density and electrostatic potential were also calculated.

Calculations of molecular interactions were done at the semiempirical level using the MOPAC2009 with the PM6 Hamiltonian and COSMO model [44] to simulate the polar environment of the molecules or ions. The "negative" of molecular surface charge density distribution, i.e. σ-profiles of the studied and model molecules and ions, was calculated by means of the COSMO-SAC model [45,46], using the COSMO files generated in the PM6/COSMO calculations with the dielectric constant $\epsilon = 1000$.

## 3. Results and discussion

### 3.1. Interactions with DNA

The first aim of the present study was to characterize the ability of the new sugar-based surfactants to interact with DNA plasmid molecules. Specifically, we intended to determine the ability of $C_n$GABs to fully compact DNA and to study the influence of their alkyl chain length on $C_n$GAB–DNA interactions.

TCSPC–FCS enables one to detect the interaction between $C_n$GAB surfactants and DNA as the mobility of a single plasmid molecule, which is assessed through its diffusion time, and the level of its compaction by particle number and lifetime changes [25]. Diffusion time and particle number are determined by fluorescence correlation spectroscopy (FCS), with fluorescence lifetime measured by time-correlated single photon counting (TCSPC).

The results of fluorescence correlation spectroscopy (TCSPC–FCS) measurements on the DNA complexes with $C_n$GAB are shown in Figs. 3–5 as the dependences of diffusion time, particle number and lifetime on $C_n$GAB/$DNA_{bp}$ ratio, respectively.

In the absence of added $C_n$GAB compounds, the free uncoiled DNA has a diffusion time of 65 ms. Within the supramolecular assembly with sugar molecules, its hydrodynamic radius becomes smaller [47] and thereby as the concentration is increased the diffusion time of plasmid DNA decreases continuously for all four $C_n$GABs. The experimental data show that the DNA molecule interacts differently with each of the four studied surfactants and the nature of this interaction depends on the length of the alkyl chain (Fig. 3). The longer the alkyl chain of the $C_n$GAB the better the interaction of the surfactant with DNA plasmid, which in consequence gives a supramolecular assembly diffusing faster. The most effective in this respect is the $C_{16}$GAB compound, which requires only 2 molecules per base pair in order to obtain a DNA molecule with the diffusion time of 4 ms. This value can be considered as the final one, at which the titration experiment indicates the formation of a globular nanoparticle. $C_{14}$GAB and $C_{12}$GAB require 20 and 200 molecules per $DNA_{bp}$, respectively, to reach that diffusion time of 4 ms; hence they are respectively 10- and 100-fold less effective. The $C_{12}$GAB surfactant shows in particular three stages of interaction with DNA. The first stage is observed for the range of $C_{12}$GAB/$DNA_{bp}$ values from 0 to 60 when the diffusion time falls to 20 ms. In the second stage, for the $C_{12}$GAB/$DNA_{bp}$ ratio from 60 to 120, no significant changes in diffusion time were observed. The third stage is observed for the $C_{12}$GAB/$DNA_{bp}$ ratio from 120 to 200, where the further increase of $C_{12}$GAB concentration causes a decrease of diffusion time to 4 ms. Increasing the $C_{10}$GAB/$DNA_{bp}$ ratio does not result in the same final diffusion time value, giving the final drop of the diffusion time to 20 ms (see Fig. 3).

Profiles of particle number (*PN*) changes closely follow the diffusion time changes (Fig. 4). The apparent particle number is a parameter related to the number of fluorescent fluctuations, and since the free multi-labeled DNA molecule is of the size of the confocal volume element, it does not reflect here the DNA concentration (which anyway is constant), but rather is related to the size of the molecule. For $C_{16}$GAB,

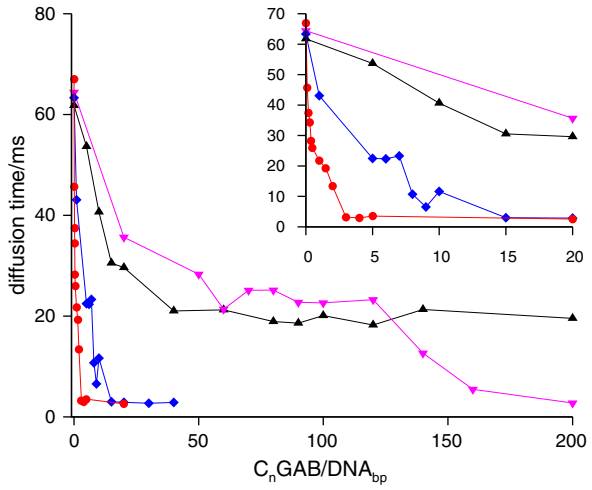


**Fig. 3.** Diffusion time as a function of $C_n$GAB to DNA base pair ratio ($C_n$GAB/$DNA_{bp}$) estimated for $n = 10$ (▲, black), 12 (▼, magenta), 14 (♦, blue) and 16 (●, red), measured in water at 25 °C. DNA was labeled with PicoGreen® (PG) with labeling ratio 2 PG/100 base pairs. The inset shows the zoomed region of $C_n$GAB/$DNA_{bp}$ ratio in the range of 0–20. Lines are included to help guide the eye.

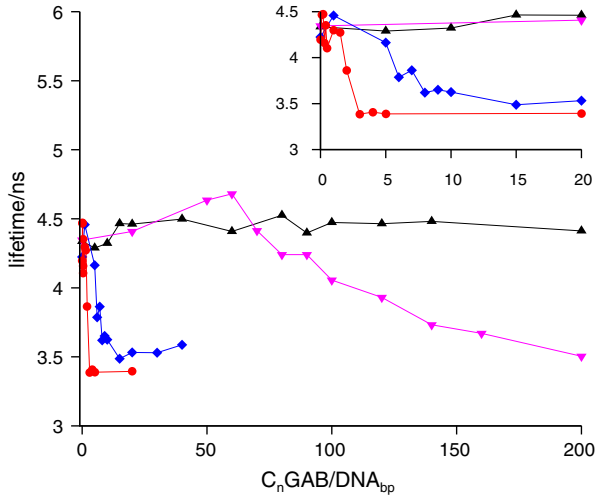


**Fig. 5.** Lifetime of PicoGreen® (PG) as a function of $C_n$GAB to DNA base pair ratio ($C_n$GAB/$DNA_{bp}$) estimated for $n = 10$ (▲, black), 12 (▼, magenta), 14 (♦, blue) and 16 (●, red), measured in water at 25 °C. Labeling ratio: 2 PG/100 base pairs. The inset shows the zoomed region of $C_n$GAB/$DNA_{bp}$ ratio in the range of 0–20. Lines are included to help guide the eye.

$C_{14}$GAB and $C_{12}$GAB a significant drop in the particle number was observed, showing that supramolecular DNA assemblies do have a considerably smaller size than the free DNA. In a model with point-like molecules at 1 nM concentration of DNA molecules the theoretical value of *PN* is around 0.6 [25]. The achieved value of *PN* was about $0.6 \pm 0.2$ at $C_n$GAB/$DNA_{bp} = 2$, 20 and 200 for DNA interacting with $C_{16}$GAB, $C_{14}$GAB and $C_{12}$GAB, respectively. This can be interpreted in such a way that in these particular FCS experiments those supramolecular assemblies do not show any segmental motion, i.e. at those $C_n$GAB concentrations the Brownian motion of fully compacted DNA is recorded. In contrast, the *PN* for $C_{10}$GAB–DNA assembly remains practically constant throughout the examined concentration range. While the modest change of the diffusion time for $C_{10}$GAB–DNA assembly indicates somewhat incomplete DNA compaction, the *PN* indicates that the addition of $C_{10}$GAB does not lead to any compaction even at high loading (ratios up to 200 $C_{10}$GAB/$DNA_{bp}$), which is also confirmed by the constant fluorescence lifetime, as discussed below.

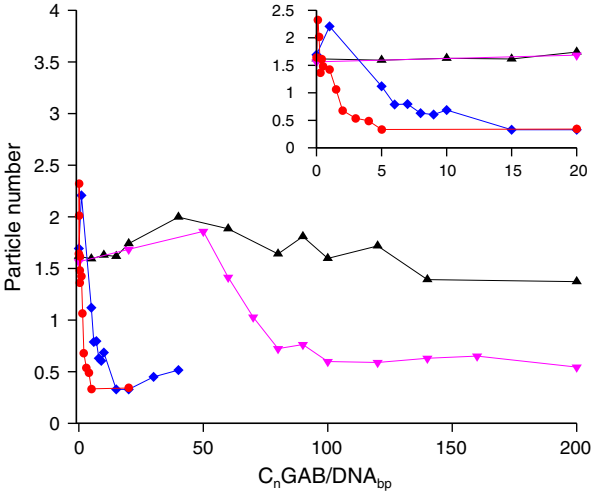


**Fig. 4.** Particle number as a function of $C_n$GAB to DNA base pair ratio ($C_n$GAB/$DNA_{bp}$) estimated for $n = 10$ (▲, black), 12 (▼, magenta), 14 (♦, blue) and 16 (●, red), measured in water at 25 °C. DNA was labeled with PicoGreen® (PG) with labeling ratio 2 PG/100 base pairs. The inset shows the zoomed region of $C_n$GAB/$DNA_{bp}$ ratio in the range of 0–20. Lines are included to help guide the eye.

Besides monitoring the classical FCS read-out parameters such as diffusion time and *PN*, we simultaneously monitored changes in the fluorescence lifetime of PicoGreen® (PG) induced by $C_n$GABs. Fluorescence lifetime of dye molecules is a sensitive reporter on the local microenvironment. A change of the immediate microenvironment of the dye molecules forces a change of its lifetime and, inversely, the lifetime remains constant under unchanged conditions [48]. In earlier studies revealing the compaction mechanism of 10 kbp DNA it was found that the lifetime of PG is $4.3 \pm 0.2$ ns for free DNA and $3.3 \pm 0.2$ ns for fully compacted DNA. For the two most effective of the studied compounds, i.e. $C_{16}$GAB and $C_{14}$GAB, increase of the $C_n$GAB/$DNA_{bp}$ ratio leads to shortening of the lifetime of PG from 4.3 ns to 3.4 ns and 3.5 ns, respectively (Fig. 5). Together with the PN values discussed above, this appears to be a clear proof that the DNA is fully compacted. On the other hand, for the $C_{10}$GAB compound no significant change in the lifetime was observed, showing no DNA compaction.

As in the case of the *PN* dependences, careful inspection of the less active $C_{12}$GAB surfactant shows some deviation from the typical concentration-dependent effect of those surfactants on DNA. Increasing the concentration of $C_{12}$GAB up to $C_{12}$GAB/$DNA_{bp} = 60$ results in an increase of the lifetime from 4.3 ns to 4.7 ns. The effect is not observed for $C_{14}$GAB and $C_{16}$GAB. Interestingly, a similar increase at the same surfactant concentration is observed for $C_{10}$GAB. The increase of the fluorescence time of PG indicates that in that concentration range both $C_{12}$GAB and $C_{10}$GAB induce a conformational change of the DNA molecule that is of opposite nature with respect to the compaction, as the latter leads to a decrease of the fluorescence lifetime. At concentrations $C_n$GAB/$DNA_{bp} > 60$, the lifetime for $C_{10}$GAB remains constant, while that for $C_{12}$GAB gradually decreases to 3.5 ns, indicating a compacted form of DNA. One can hypothesize that this increase of the lifetime may be due to discrete conformational transition of DNA from loosely packed spherical through toroidal to rod-like, with increasing surfactant concentration below its critical micelle concentration (CMC), as reported for cetyltrimethylammonium bromide (CTAB), inducing changes in the form of aggregated DNA molecules [49]. The CMCs of $C_n$GABs, pre-determined at 25 °C using the isothermal titration calorimetry method, take values of about 90 mM, 27 mM, 6 mM and 1 mM for $n = 10$, 12, 14 and 16 respectively [50]. In the experiments

on $C_n$GAB–DNA interactions reported above, the maximum surfactant concentrations of 2 mM for $C_{10}$GAB and $C_{12}$GAB, 0.4 mM for $C_{14}$GAB and 0.2 mM for $C_{16}$GAB were used. Thus, the observed DNA compaction occurs at surfactant concentrations below the critical micellar concentrations. This means that the observed DNA compaction phenomenon involves single surfactant molecules rather than micelles.

In summary, the experimental results for these three parameters (diffusion time, particle number and lifetime) show that $C_{12}$GAB, $C_{14}$GAB and $C_{16}$GAB are able to fully condense DNA. Even high concentrations of $C_{10}$GAB do not lead to a comparable effect. The obtained data indicate that low concentrations of $C_{10}$GAB lead to a remarkable conformational change of the DNA molecule, of significantly different nature than the compaction process. Higher concentration does not transform this supramolecular assembly to a condensed DNA nanoparticle. Classification of the capacity of $C_n$GAB to interact with DNA can be made in the following order: $C_{16}$GAB > $C_{14}$GAB > $C_{12}$GAB. The latter shows the peculiarity that at lower concentrations (prior to DNA compaction) a conformational change of DNA is induced, similar to that observed for $C_{10}$GAB. An increment by 2 carbon atoms in the alkyl chain (from 12 to 14 to 16) results in a drop in the value of the $C_n$GAB/$DNA_{bp}$ ratio required for the DNA compaction by an order of ten (200, 20 and 2, respectively), which is in agreement with the observed dependence of DNA condensation ability on the number of carbon atoms in homologous series of cationic surfactants [51]. For $C_{16}$GAB the process is most efficient, taking place at the ratio $C_{16}GAB/DNA_{bp} = 2$, i.e. the concentration of one surfactant molecule per nucleotide. This suggests that each $C_{16}GA^+$ cation neutralizes one negatively charged phosphate group of DNA backbone and its alkyl tail is sufficiently long to collectively promote the process of DNA coil-to-globule transformation.

Results from previous work, obtained from ultra-sensitive techniques based on the detection of single molecules, optical tweezers and fluorescence lifetime correlation spectroscopy (FLCS) [52,53] for CTAB, show that compaction occurred for $CTAB/DNA_{bp} = 4$. The single-molecule experiments (TCSPC–FCS) presented here demonstrate that $C_{16}$GAB surfactant monomers are indeed able to bind and compact plasmid DNA at concentrations twice as low as for a typical cationic surfactant, CTAB.

The mechanism of interaction of DNA with surfactants is still under discussion. The fluorescence lifetime correlation studies show that surfactants compact DNA in a rather continuous manner, while in the case of multivalent cations missing hydrophobic tails, i.e. when compaction is driven electrostatically, the process occurs in the none-or-all mode [24,27]. Apparently, $C_{16}$GAB and $C_{14}$GAB bound to the DNA molecule are subject to strong cooperative binding due to the hydrophobic attraction of alkyl tails of surfactants. The increase of local amphiphile density results in a charge inversion of a DNA segment and leads to the partial compaction of the DNA. In other words, when the number of adjacent neutralized segments is sufficiently high, the hydrophobic interactions of the tails cause the partial collapse of the neutralized domain independently of the rest of the DNA molecule. With increasing amounts of $C_{16}$GAB and $C_{14}$GAB, more and more domains are collapsed, and eventually the entire DNA molecule becomes compacted. The hypothesis is based on the FLCS studies on CTAB surfactant [53] and is in agreement with the reported effect of interchain segregation during the DNA compaction process [54,55], indicating that DNA molecules can collapse in separated domains. On the other hand, the interactions between the hydrophobic chains of $C_{10}$GAB are not strong enough to favor such cooperative binding. $C_{10}$GAB binds randomly to the DNA molecule and thus does not lead to an elevated local amphiphile density. The resulting charge inversion by the randomly bound monovalent cations is insufficient to cause electrostatically driven DNA compaction. $C_{12}$GAB shows the latter binding mode at lower $C_{12}GAB/DNA_{bp}$ values. However, at higher concentrations the local density of interacting hydrophobic chains is high enough to switch to the cooperative binding mode observed for $C_{14}$GAB and $C_{16}$GAB.

### 3.2. Interactions with model lipid membrane

Interactions of $C_n$GAB with dipalmitoylphosphatidylcholine bilayer were investigated by means of differential scanning calorimetry and fluorescence spectroscopy. The phase behavior and membrane fluidity changes induced by $C_n$GABs were analyzed at a concentration of surfactants in the lipid bilayer of 10 mol% using three fluorescent probes.

The packing order of the hydrophilic region of DPPC lipid membranes was investigated using Prodan and Laurdan. Laurdan is a membrane fluorescent probe that has the unique advantage of being sensitive to the phospholipid phase state. It is located in the hydrophilic–hydrophobic interface of the bilayer with the lauric acid tail anchored in the phospholipid acyl chain region [56]. Compared to Laurdan, Prodan has different location in a lipid membrane, namely closer to the aqueous phase. Such a location allows Prodan to be sensitive also to the pre-transition occurring in the region of lipid headgroups [31,32].

Generalized polarization (*GP*) of Prodan and Laurdan was measured for pure DPPC and DPPC-$C_n$GAB systems. *GP* of Prodan in SUVs formed from DPPC is presented in Fig. 6A as a function of temperature. Presence of $C_n$GAB has an impact on temperature of the pre-transition of DPPC but does not eliminate it. The results indicate that major changes caused by the compounds appear in the gel-like crystalline phase of a DPPC bilayer. The largest effects on the pre-transition are present for $C_{14}$GAB and $C_{16}$GAB. It is interesting that $C_{10}$GAB slightly increases *GP*, which indicates increasing order in the hydrophilic region of the lipid bilayer and presence of the compound in that area.

For Laurdan (Fig. 6B) changes in *GP* are strongest in the presence of $C_{14}$GAB, both in the gel and liquid-crystalline phases. $C_{14}$GAB also causes the most pronounced decrease of the main phase transition temperature $T_m$. Smaller changes were observed in the main phase transition temperature in the presence of other compounds being investigated. In general, the values of *GP* slightly decrease with the presence of the surfactants, which indicates increasing disorder in the hydrophilic–hydrophobic interface of the DPPC bilayer and presence of the compounds in that region.

The effect of the surfactant on the fluidity of the membrane was studied on the basis of fluorescence anisotropy measured with the DPH probe, which is located in the hydrophobic region of the bilayer. The DPH steady-state anisotropy is primarily related to the restriction of the rotational motion of the probe due to the hydrocarbon chain packing order. Therefore the decrease of the parameter can be explained by the structural perturbation of the bilayer hydrophobic region due to the incorporation of studied compounds [57]. The observed dependence of the DPH probe on temperature is presented in Fig. 6C, showing that the effect of the presence of any of the investigated compounds on the fluorescence anisotropy is in general very small, being most apparent for $C_{14}$GAB.

The effects of $C_n$GABs on the phase transition of DPPC determined in the DSC experiments are shown in Figs. 7 and 8, and in Table 1. In order to elucidate the interactions of the surfactants with a DPPC membrane one can consider a dual behavior of the surfactants related to their chemical structure. The interactions of the gluconamide moiety with the DPPC headgroup are similar to those of glucose, forming hydrogen bonds with the phosphate and ester groups of the DPPC molecule, which leads to the stiffening of the bilayer structure [58]. In turn, the effect of the remainder of the $C_nGA^+$ cation is similar to that of $C_n$TABs, i.e. it causes the loosening of the membrane structure. With an increase of the alkyl chain length the second effect should be more pronounced.

For $C_{10}$GAB the first effect prevails as can be seen from the slight increase of *GP* in the gel phase for Prodan (Fig. 6A) and virtually no effect on $T_m$ up to molar ratio 0.2 (Fig. 9), although it raises $\Delta H_m$. This indicates stiffening of the membrane in the surface layer. The pre-transition also was affected only a little (see Fig. 7). The transition peaks were broader and asymmetrical at molar ratios higher than

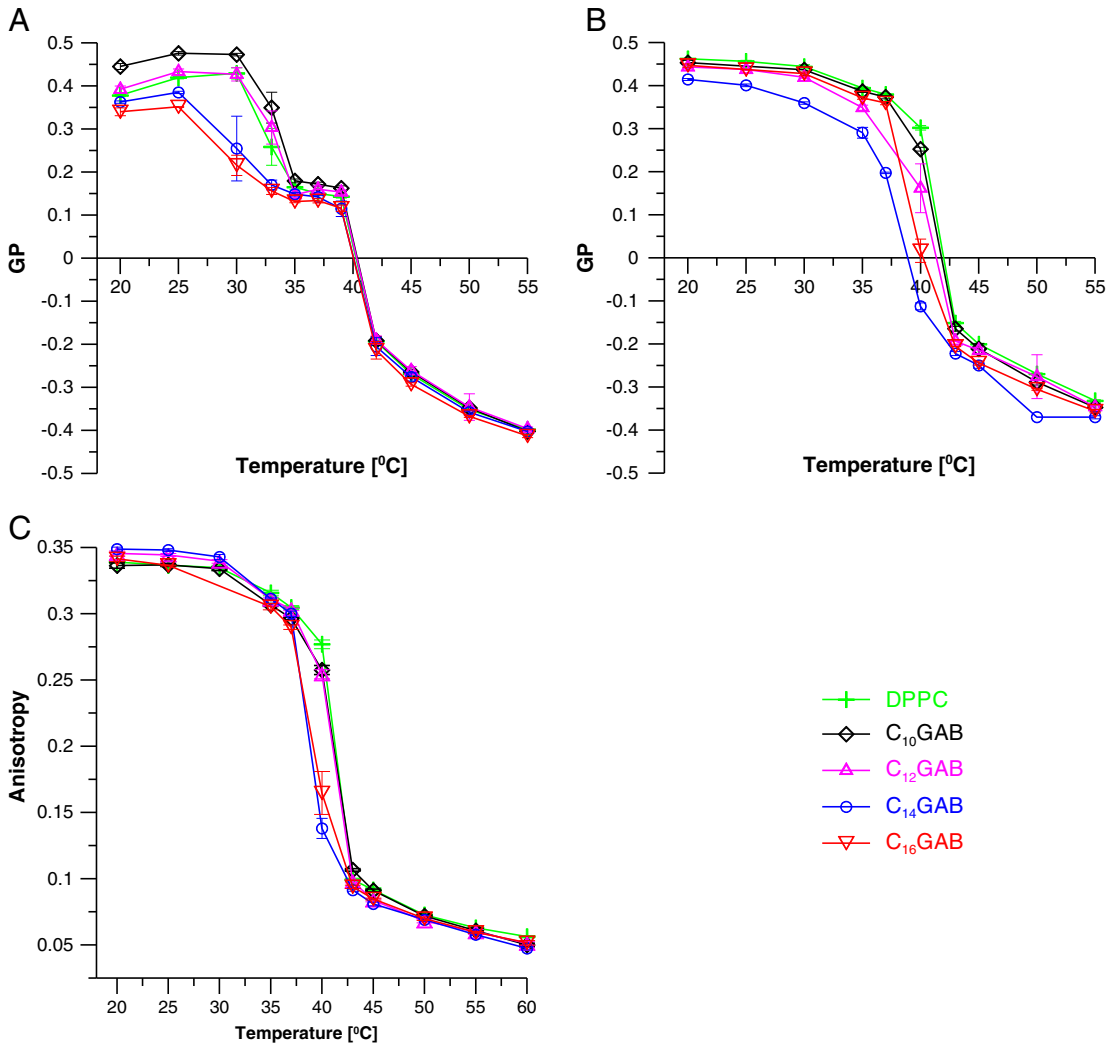


**Fig. 6.** Values of general polarization of Prodan (A) and Laurdan (B) and fluorescence anisotropy of DPH (C) in SUVs formed from DPPC in the absence and presence of $C_nGAB$ ($n$ = 10, 12, 14, 16) as a function of temperature. Molar ratio $C_nGAB$/DPPC = 0.1. Lines are included to help guide the eye.

0.18. These results suggest that $C_{10}GAB$ does not significantly change the structure and organization of the phospholipid bilayer. It seems to be slightly active only at high concentrations. $C_{12}GAB$ and $C_{14}GAB$, having longer tails, show a stronger fluidization effect, apparent in lowering $T_m$. The DSC curves (Fig. 7) are symmetrical, which suggests uniform location of the compounds in the gel phase of the liposomes.

In the case of $C_{16}GAB$ most interesting effects were observed. Its fluidization effect is weaker than for $C_{12}GAB$ and $C_{14}GAB$, as was observed for surfactants with tail length equal to or longer than palmitoyl chains of DPPC [59]. As can be seen in Fig. 7, starting at the compound-to-lipid ratio of 0.1 the main phase transition peak separates into two components. The temperature of the first component (marked I in Fig. 7) is approximately the same as $T_m$ for pure DPPC. The second component (marked II) was assigned to the temperature of the main phase transition of the mixed bilayer and therefore taken into account in the chart in Fig. 8. $C_{16}GAB$ lowers $T_m$ but less than $C_{12}GAB$ and $C_{14}GAB$, and raises $\Delta H_m$. Moreover, a shoulder arises on the DSC curves. The possible interaction with the headgroup of DPPC may be supported by the effect of the compounds on the pre-transition, shown in Fig. 6A. These interactions may also cause an increase in $\Delta H_m$. Therefore, the effect of the gluconamide moiety of $C_{16}GAB$ seems to be more pronounced than in the case of $C_{12}GAB$ and $C_{14}GAB$. It may also lead to phase separation, in agreement with the hypothesis by Jain and Wu [60] that the compound specifically interacting with the polar headgroup of DPPC promotes phase separation.

The strongest fluidization effect on the membrane is shown by the $C_{14}GAB$ compound, as is apparent from the lowering of *GP* for the Laurdan probe (Fig. 6B) and the fall in the phase transition temperature (Fig. 9). Anyway, it is worth noting that in general the effect of $C_nGABs$ on the main phase transition in the DPPC bilayer is much weaker than in the case of standard cationic surfactants of the same alkyl tail length such as $C_nTABs$ [30], *n*-alkyl-N,N-dimethyl-N-benzylammonium bromides ($C_nBeABs$) [28], and even the glucocationic bromides $C_nAGCBs$ studied by Fisicaro et al. [14]. One can hypothesize that the stronger fluidization effect of the latter compounds is related to the weaker hydrogen bonding ability of their headgroups with the polar part of DPPC.

### 3.3. Modeling studies

The DPPC molecule and $C_nGA^+$ cations were modeled on the classical and quantum-mechanical level, to reveal which of their molecular properties affect interactions and behavior of the studied systems observed in experiments. Studies of the conformational space of the molecules were done by means of classical simulated annealing molecular dynamics with the alkyl or acyl chains fixed in the all-trans

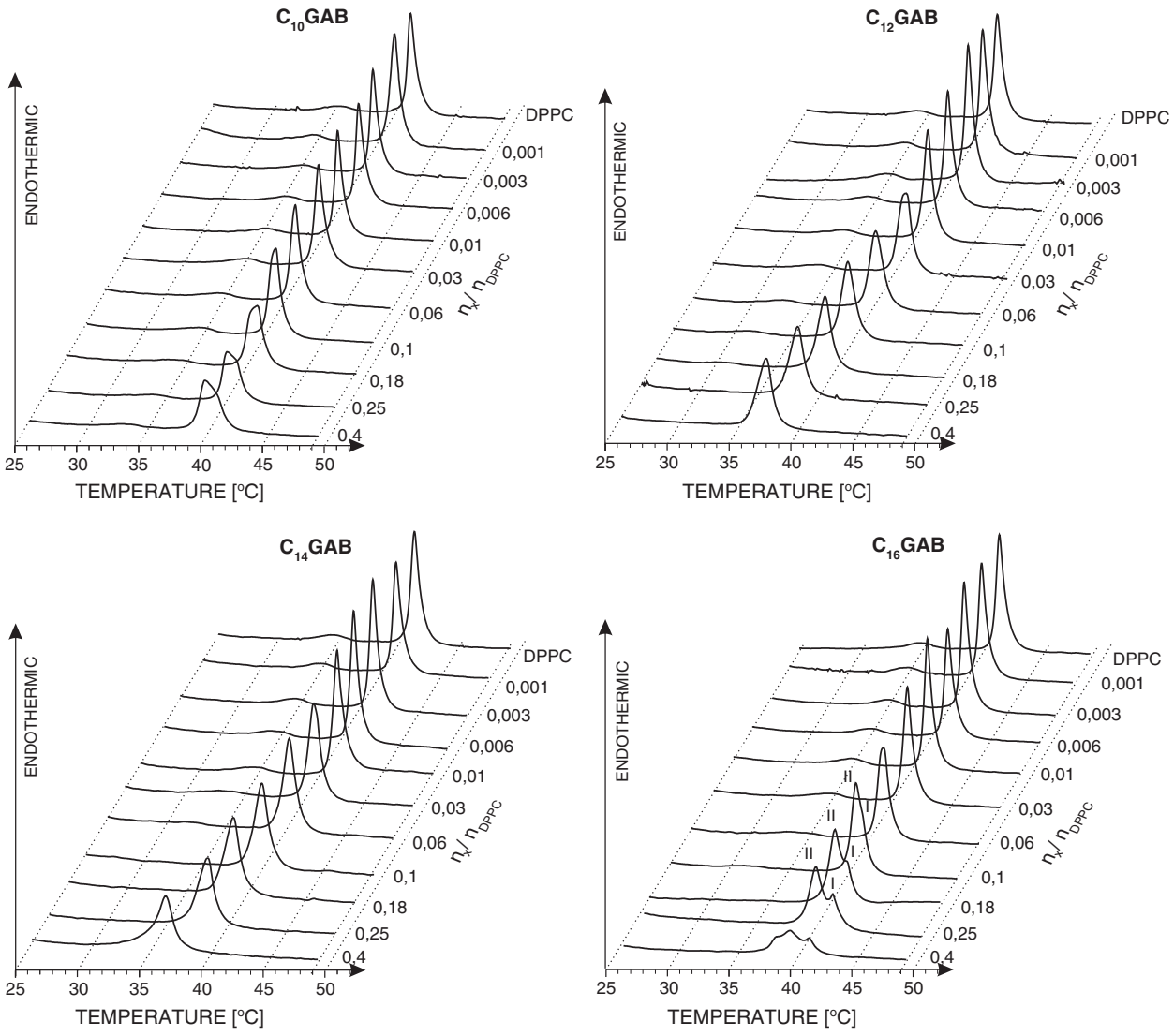


**Fig. 7.** DSC heating curves of MLVs with increasing molar ratios of $C_n$GABs ($n$ = 10, 12, 14, 16) to DPPC. The curves are normalized for the amount of DPPC; scan rate 2 °C/min.

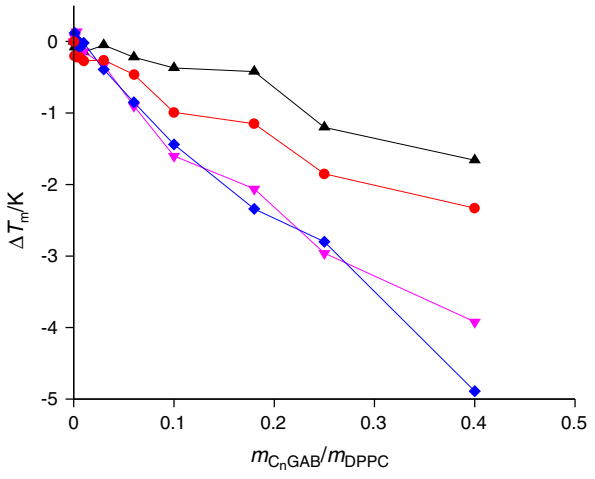


**Fig. 8.** Change of the temperature of the main phase transition $T_m$ in the lipid bilayer modified with $C_n$GAB with respect to the pure DPPC bilayer, $\Delta T_m = T_m - 41.35$ °C vs. surfactant-to-lipid molar ratio $m_{CnGAB}/m_{DPPC}$ for $n$ = 10 (▲, black), 12 (▼, magenta), 14 (◆, blue) and 16 (●, red). Lines are included to help guide the eye.

conformation, followed by the unconstrained quantum-mechanical geometry optimization of the few lowest-energy conformations. Examples of the final optimized conformations are shown in Fig. 9. It is worth noting that all lowest-energy surfactant cation conformations show the

**Table 1**
Temperature $T_m$ and enthalpy change $\Delta H$ of the main phase transition of the lipid bilayer vs. surfactant-to-lipid molar ratio ($m_{CnGAB}/m_{DPPC}$) for $n$ = 10, 12, 14 and 16.

| $m_{CnGAB}/m_{DPPC}$ | $C_{10}$GAB | | $C_{12}$GAB | | $C_{14}$GAB | | $C_{16}$GAB | |
|---|---|---|---|---|---|---|---|---|
| | $T_m$/°C | $\Delta H$/(kJ/mol) | $T_m$/°C | $\Delta H$/(kJ/mol) | $T_m$/°C | $\Delta H$/(kJ/mol) | $T_m$/°C | $\Delta H$/(kJ/mol) |
| 0.000 | 41.35 | 36.4 | 41.35 | 36.4 | 41.35 | 36.4 | 41.35 | 36.4 |
| 0.001 | 41.27 | 35.3 | 41.41 | 37.6 | 41.47 | 32.0 | 41.15 | 36.6 |
| 0.003 | 41.27 | 35.5 | 41.49 | 38.0 | 41.38 | 32.8 | 41.13 | 37.6 |
| 0.006 | 41.30 | 36.0 | 41.34 | 36.0 | 41.26 | 33.8 | 41.13 | 37.7 |
| 0.010 | 41.20 | 34.7 | 41.21 | 36.3 | 41.33 | 34.0 | 41.08 | 38.1 |
| 0.030 | 41.30 | 40.3 | 41.02 | 35.8 | 40.96 | 34.5 | 41.09 | 38.3 |
| 0.060 | 41.13 | 39.1 | 40.45 | 32.7 | 40.50 | 34.9 | 40.89 | 37.8 |
| 0.100 | 40.98 | 41.8 | 39.75 | 34.6 | 39.91 | 34.3 | 40.36[a] | 39.3 |
| 0.180 | 40.93 | 35.7 | 39.29 | 34.6 | 39.01 | 34.1 | 40.20[a] | 39.6 |
| 0.250 | 40.15 | 33.3 | 38.39 | 34.5 | 38.55 | 33.9 | 39.50[a] | 40.7 |
| 0.400 | 39.69 | 34.3 | 37.43 | 34.4 | 36.46 | 33.2 | 39.02 | 36.5 |

[a] The values for the peaks marked II in DSC thermograms, i.e. related to the $C_{16}$GAB-rich domains in the DPPC membrane.

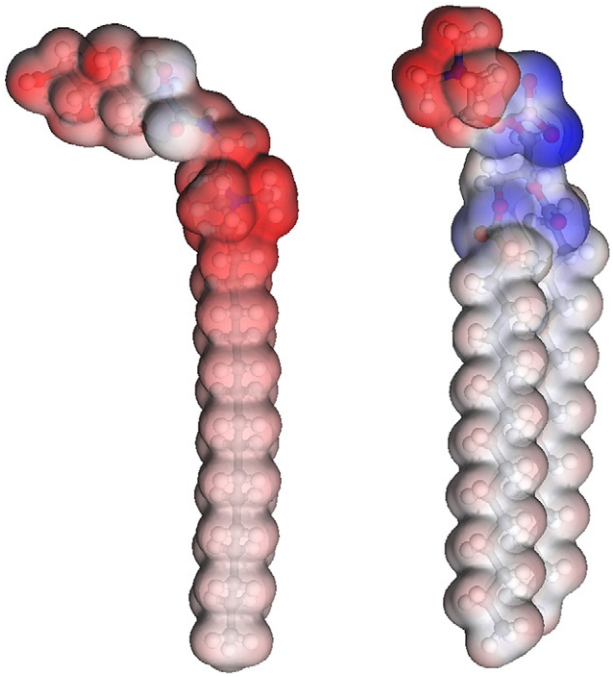

**Fig. 9.** Picture of $C_{16}GA^+$ (left) and DPPC (right) both with alkyl chains in all-trans conformation. Electron density surfaces covering the ball-and-stick models are colored according to the local molecular electrostatic potential; blue — negative, red — positive.

"bent" structure, i.e. the headgroup is tilted with respect to the direction determined by the alkyl tail. Similar tilt appears in the DPPC molecules in the bilayer in gel and liquid-crystalline phase.

The differences in the effects on DPPC membrane between $C_{16}GAB$ and its analogs with a shorter alkyl tail can be elucidated, at least qualitatively, based on the molecular structure. $C_nGABs$ have a large headgroup, similar in size to the hydrophilic part of DPPC, and $C_{16}GAB$ also has a hydrophobic tail long enough to be commensurate with the palmitoyl tails of the DPPC molecule, as can be seen in Fig. 10. Besides, the distribution of electrostatic potential on the molecular surfaces favors the alignment of the surfactant and lipid molecules in such a way that the quaternary nitrogen of the surfactant tends to be close to the phosphate of the lipid. In other words, positively charged regions

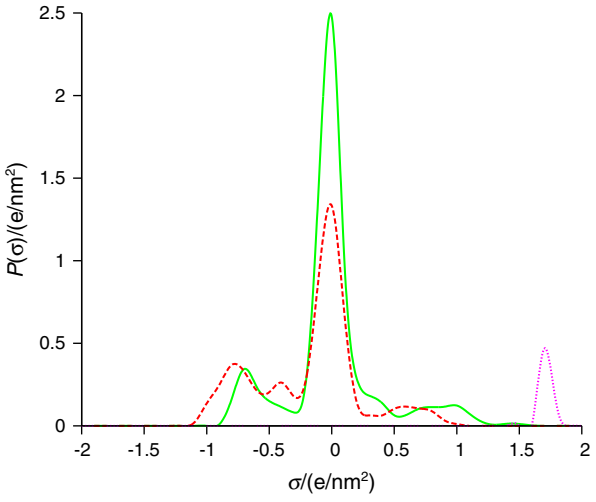


**Fig. 10.** The σ-profiles of DPPC molecule (green, solid line), $C_{16}GA^+$ cation (red, dashed line) and $Br^-$ anion (magenta, dotted line) generated using MOPAC2009 PM6 and COSMO-SAC model.

on the surfactant cation surface (red surface regions in Fig. 10; more intense color means higher electrostatic potential), especially those around the ammonium group, "fit" the region of the most negative electrostatic potential (blue surface regions in Fig. 9; more intense color means a more negative value) surrounding mainly the phosphate group of the DPPC headgroup, while the aligned tails of both species may participate in hydrophobic interactions.

The hydrophilic part of $C_nGABs$ has six polar groups able to form hydrogen bonds. Hydroxyl groups of the gluconamide moiety can form intramolecular bonds, but there still remain H-bond donors and acceptors that could be hydrogen-bonded to the neighboring water or other molecules. One can thus expect the headgroups of $C_nGABs$ to form hydrogen bonds with lipid headgroups, partially reducing the water shell surrounding both the surfactants' and lipids' polar parts [58].

One can thus suppose that the $C_{16}GAB$ moiety built into the DPPC membrane fits the surrounding lipid molecules quite well in the headgroups as well as in the hydrophobic tail regions, and in effect only moderately disturbs the bilayer structure even in the surfactant-rich domains. $C_{12}GAB$ and $C_{14}GAB$, interacting in the same way with the lipid headgroups, intercalate the lipid bilayer and disturb its structure due to the incommensurability of their alkyl tails and the acyl chains of DPPC molecules. This leads to easier liquidization of the lipid bilayer, i.e. a more pronounced fall in the $T_m$.

The molecular σ-profiles were used for qualitative explanation of interactions between the molecules. The σ-profiles of the DPPC molecule, $C_{16}GA^+$ cation and $Br^-$ anion are shown in Fig. 10. The shape of the negative shoulder of the $C_{16}GA^+$ σ-profile indicates that the positive charge of the cation is strongly delocalized. As can be seen in Fig. 9, the positive electrostatic potential is spread from the amine group to the third methylene group of the alkyl tail. In the DPPC molecule the positive charge is much more localized, as the positive potential appears only on the trimethylammonium group.

The strong shoulder for the negative $\sigma$ in the $C_{16}GA^+$ profile and the broad shoulder for the positive $\sigma$ of the DPPC profile indicate the possibility of relatively strong electrostatic interactions between the positively charged regions of the headgroup of $C_nGAB$ and the negatively charged phosphate group of DPPC. The σ-profile of the $C_{16}GA^+$ cation alone also suggests the possibility of local attractive interactions between polarized headgroups, in addition to the general electrostatic repulsion of like charges. The significant number of hydrogen bond donors and acceptors in the headgroup allows the formation of many H-bonds, both intramolecular and intermolecular, with the lipid molecules and surrounding water as well as between surfactants.

Accounting for the possible electrostatic interactions and hydrogen bonding together with the commensurability of the hydrophobic tail of $C_{16}GA^+$ with acyl chains of DPPC, one can support the explanation of a weaker effect of $C_{16}GAB$ than $C_{12}GAB$ and $C_{14}GAB$ on the phase transitions in lipid bilayers. In turn, the possible interactions between surfactant headgroups together with hydrophobic interactions of the tails, the stronger the longer the alkyl chain, support the presumed formation of surfactant-rich domains at higher concentrations of $C_{16}GAB$ in the DPPC bilayer.

## 4. Conclusions

The series of four novel glucose-derived cationic surfactants, $C_nGAB$, prepared according to green chemistry methods, was studied with respect to the interactions with DNA and model lipid membrane in view of potential gene-delivery applications. Spectroscopic and calorimetric experimental methods were involved and theoretical methods were used to support the interpretation of experimental results at the molecular level.

The results show that the ability to compact plasmid DNA rises exponentially with the surfactant alkyl chain length and for $C_{16}GAB$ the concentration inducing full compaction is close to one surfactant

molecule per nucleotide, i.e. per DNA phosphate group. $C_{16}$GAB is thus quite an effective DNA-compacting agent, both due to the appropriate hydrophobic chain length and due to the large polar headgroup. While binding to DNA, not only do the surfactant cations almost fully neutralize the negative charge of the DNA backbone but also it is likely that the headgroup of the surfactant interacts with the relatively hydrophilic DNA surface, while the long hydrophobic tails promote the cooperative binding and hence compaction of the DNA [51].

Measurements show that the compounds interact with the DPPC membrane differently, depending on the length of the hydrophobic tail. $C_{12}$GAB and $C_{14}$GAB lower the main phase transition temperature of DPPC more than $C_{10}$GAB and $C_{16}$GAB. $C_{16}$GAB induces the formation of surfactant-rich and surfactant-poor domains in the membrane starting from a molar surfactant-to-DPPC ratio of about 0.1. Moreover, the chemical structure of the presented glucose-derived surfactants favors hydrogen bonding of $C_n$GAB and DPPC headgroups, as in the case of sugars, which weakens the destructive effect on the membrane compared to linear cationic surfactants with the same aliphatic tails.

In summary, $C_{16}$GAB seems to be a promising candidate for a main component of gene-delivery carrier systems. The compound compacts DNA at concentrations as low as 1:1 surfactant-to-nucleotide ratio, and only very slightly disturbs the lipid membrane structure, even when forming domains at concentrations in the lipid phase at 10 mol% and up, as follows from the slight decrease of $T_m$. We hypothesize that the observed formation of surfactant-rich membrane domains might facilitate passing the condensed DNA-containing vectors through the membrane in the course of endocytosis.

## Acknowledgments

This work was supported by grant N N305 361739 from the Polish Ministry of Science and Higher Education.

Martin Hof acknowledges support from the Czech Science Foundation via grant P208/12/G016 and the Praemium Academiae Award (Academy of Sciences of the Czech Republic). Teresa Kral acknowledges the MEYS ESF Project CZ.1.07/2.3.00/20.0092.

The use of a DSC in the Institute of Agricultural Engineering of Wrocław University of Environmental and Life Sciences is gratefully acknowledged.

The modeling computations were, in part, performed using the software and the computing resources provided by the Wroclaw Centre for Networking and Supercomputing (WCSS).

## References

[1] B. Lindman, K. Thalberg, in: E.D. Goddard, K.P. Ananthapadamanabhan (Eds.), Interactions of Surfactants with Polymers and Proteins, CRC Press, Boca Raton, FL, 1993, pp. 203–276.
[2] V. Labhasetwar, Nanotechnology for drug and gene therapy: the importance of understanding molecular mechanisms of delivery, Current Opinion in Biotechnology 16 (2005) 674–680.
[3] M.L. Read, A. Logan, L.W. Seymour, Barriers to gene delivery using synthetic vectors, Advances in Genetics 53PA (2005) 19–46.
[4] E. Wagner, M. Cotten, R. Foisner, M.L. Birnstiel, Transferrin-polycation–DNA complexes: the effect of polycations on the structure of the complex and DNA delivery to cells, Proceedings of the National Academy of Sciences of the United States of America 88 (1991) 4255–4259.
[5] M. Köping-Höggård, Y.S. Mel'nikova, K.M. Vårum, B. Lindman, P. Artursson, Relationship between the physical shape and the efficiency of oligomeric chitosan as a gene delivery system in vitro and in vivo, The Journal of Gene Medicine 5 (2003) 130–141.
[6] M. Morille, C. Passirani, A. Vonarbourg, A. Clavreul, J.-P. Benoit, Progress in developing cationic vectors for non-viral systemic gene therapy against cancer, Biomaterials 29 (2008) 3477–3496.
[7] A.N. Zelikin, A.L. Becker, A.P.R. Johnston, K.L. Wark, F. Turatti, F. Caruso, A general approach for DNA encapsulation in degradable polymer microcapsules, ACS Nano 1 (2007) 63–69.
[8] D.D. Lasic, H. Strey, M.C.A. Stuart, R. Podgornik, P.M. Frederik, The structure of DNA–liposome complexes, Journal of the American Chemical Society 119 (1997) 832–833.
[9] C.-Y. Huang, T. Uno, J.E. Murphy, S. Lee, J.D. Hamer, J.A. Escobedo, et al., Lipitoids — novel cationic lipids for cellular delivery of plasmid DNA in vitro, Chemistry & Biology 5 (1998) 345–354.
[10] Y. Zhou, Y. Li, Studies of interaction between poly(allylamine hydrochloride) and double helix DNA by spectral methods, Biophysical Chemistry 107 (2004) 273–281.
[11] A. Colomer, A. Pinazo, M.T. García, M. Mitjans, M.P. Vinardell, M.R. Infante, et al., pH-sensitive surfactants from lysine: assessment of their cytotoxicity and environmental behavior, Langmuir 28 (2012) 5900–5912.
[12] J.J. McManus, J.O. Rädler, K.A. Dawson, Does calcium turn a zwitterionic lipid cationic? The Journal of Physical Chemistry. B 107 (2003) 9869–9875.
[13] J.J. McManus, J.O. Rädler, K.A. Dawson, Observation of a rectangular columnar phase in a DNA–calcium–zwitterionic lipid complex, Journal of the American Chemical Society 126 (2004) 15966–15967.
[14] E. Fisicaro, C. Compari, M. Biemmi, E. Duce, M. Peroni, G. Donofrio, et al., Thermodynamics and biological properties of the aqueous solutions of new glucocationic surfactants, The Journal of Physical Chemistry. B 112 (2008) 9360–9370.
[15] U. Bazylińska, R. Skrzela, K. Szczepanowicz, P. Warszyński, K.A. Wilk, Novel approach to long sustained multilayer nanocapsules: influence of surfactant head groups and polyelectrolyte layer number on the release of hydrophobic compounds, Soft Matter 7 (2011) 6113–6124.
[16] K.A. Wilk, K. Zielińska, A. Hamerska-Dudra, A. Jezierski, Biocompatible microemulsions of dicephalic aldonamide-type surfactants: formulation, structure and temperature influence, Journal of Colloid and Interface Science 334 (2009) 87–95.
[17] K.A. Wilk, K. Zielińska, J. Pietkiewicz, N. Skołucka, A. Choromańska, J. Rossowska, et al., Photo-oxidative action in MCF-7 cancer cells induced by hydrophobic cyanines loaded in biodegradable microemulsion-templated nanocapsules, International Journal of Oncology 41 (2012) 105–116.
[18] U. Laska, K.A. Wilk, I. Maliszewska, L. Syper, Novel glucose-derived gemini surfactants with a 1,1′-ethylenebisurea spacer: preparation, thermotropic behavior, and biological properties, Journal of Surfactants and Detergents 9 (2006) 115–124.
[19] P.C. Bell, M. Bergsma, I.P. Dolbnya, W. Bras, M.C.A. Stuart, A.E. Rowan, et al., Transfection mediated by gemini surfactants: engineered escape from the endosomal compartment, Journal of the American Chemical Society 125 (2003) 1551–1558.
[20] N. Adjimatera, A. Benda, I.S. Blagbrough, M. Langner, M. Hof, T. Kral, Fluorescence correlation spectroscopic studies of a single lipopolyamine–DNA nanoparticle, in: M.N. Berberan-Santos (Ed.), Fluorescence of Supermolecules, Polymers, and Nanosystems, Springer, Berlin/Heidelberg, 2008, pp. 381–413.
[21] A. Benda, M. Hof, M. Wahl, M. Patting, R. Erdmann, P. Kapusta, TCSPC upgrade of a confocal FCS microscope, The Review of Scientific Instruments 76 (2005), (033106-1-4).
[22] T. Kral, J. Leblond, M. Hof, D. Scherman, J. Herscovici, N. Mignet, Lipopolythiourea/DNA interaction: a biophysical study, Biophysical Chemistry 148 (2010) 68–73.
[23] D. Magde, E.L. Elson, W.W. Webb, Fluorescence correlation spectroscopy. II. An experimental realization, Biopolymers 13 (1974) 29–61.
[24] J. Humpolíčková, A. Benda, J. Sýkora, R. Machán, T. Kral, B. Gasinska, et al., Equilibrium dynamics of spermine-induced plasmid DNA condensation revealed by fluorescence lifetime correlation spectroscopy, Biophysical Journal 94 (2008) L17–L19.
[25] N. Adjimatera, T. Kral, M. Hof, I. Blagbrough, Lipopolyamine-mediated single nanoparticle formation of calf thymus DNA analyzed by fluorescence correlation spectroscopy, Pharmaceutical Research 23 (2006) 1564–1573.
[26] R. Winkler, S. Keller, J. Rädler, Intramolecular dynamics of linear macromolecules by fluorescence correlation spectroscopy, Physical Review E 73 (2006) 41919.
[27] J. Humpolíčková, M. Stepánek, T. Kral, A. Benda, K. Procházka, M. Hof, On mechanism of intermediate-sized circular DNA compaction mediated by spermine: contribution of fluorescence lifetime correlation spectroscopy, Journal of Fluorescence 18 (2008) 679–684.
[28] B. Różycka-Roszak, A. Przyczyna, Interaction between N-dodecyl-N, N-dimethyl-N-benzylammonium halides and phosphatidylcholine bilayers — the effect of counterions, Chemistry and Physics of Lipids 123 (2003) 209–221.
[29] E. Fisicaro, C. Compari, E. Duce, G. Donofrio, B. Różycka-Roszak, E. Woźniak, Biologically active bisquaternary ammonium chlorides: physico-chemical properties of long chain amphiphiles and their evaluation as non-viral vectors for gene delivery, Biochimica et Biophysica Acta, General Subjects 1722 (2005) 224–233.
[30] B. Różycka-Roszak, H. Pruchnik, Effect of counterions on the influence of dodecyltrimethylammonium halides on thermotropic phase behaviour of phosphatidylcholine bilayers, Zeitschrift fur Naturforschung. Section C. Journal of Biosciences 55 (2000) 240–244.
[31] T. Parasassi, E.K. Krasnowska, L.A. Bagatolli, Laurdan and Prodan as polarity-sensitive fluorescent membrane probes, Journal of Fluorescence 8 (1998) 365–373.
[32] E.K. Krasnowska, L.A. Bagatolli, E. Gratton, T. Parasassi, Surface properties of cholesterol-containing membranes detected by Prodan fluorescence, Biochimica et Biophysica Acta — Biomembranes 1511 (2001) 330–340.
[33] J.R. Lakowicz, Fluorescence anisotropy, Principles of Fluorescence Spectroscopy, Springer, New York, 2006, pp. 353–382.
[34] Materials Studio Release Notes, Release 6.0, Accelrys Software Inc., San Diego, 2012.
[35] J.J.P. Stewart, MOPAC2009, MOPAC2009, Stewart Computational Chemistry, Version 11.366W. Web: http://openmopac.net.
[36] A. Pedretti, L. Villa, G. Vistoli, VEGA — an open platform to develop chemo-bioinformatics applications, using plug-in architecture and script programming, Journal of Computer-Aided Molecular Design 18 (2004) 167–173.
[37] B. Różycka-Roszak, P. Misiak, E. Woźniak, A. Mozrzymas, Z. Dega-Szafran, Calorimetric and molecular modeling studies of N-alkoxycarbonylmethyl-N-alkylpiperidinium chlorides, Colloids and Surfaces A: Physicochemical and Engineering Aspects 318 (2008) 301–306.
[38] B. Różycka-Roszak, P. Misiak, B. Jurczak, K.A. Wilk, Aggregation studies of n-alkanoyl-N-methyllactitolamine surfactants, The Journal of Physical Chemistry. B 112 (2008) 16546–16551.

[39] B. Delley, An all-electron numerical method for solving the local density functional for polyatomic molecules, The Journal of Chemical Physics 92 (1990) 508–517.
[40] B. Delley, Ground-state enthalpies: evaluation of electronic structure approaches with emphasis on the density functional method, The Journal of Physical Chemistry. A 110 (2006) 13629–13632.
[41] S.H. Vosko, L. Wilk, M. Nusair, Accurate spin-dependent electron liquid correlation energies for local spin density calculations: a critical analysis, Canadian Journal of Physics 58 (1980) 1200–1211.
[42] A.D. Becke, A multicenter numerical integration scheme for polyatomic molecules, The Journal of Chemical Physics 88 (1988) 2547–2553.
[43] J.P. Perdew, Y. Wang, Accurate and simple analytic representation of the electron-gas correlation energy, Physics Review B 45 (1992) 13244–13249.
[44] A. Klamt, G. Schüürmann, COSMO: a new approach to dielectric screening in solvents with explicit expressions for the screening energy and its gradient, Journal of the Chemical Society, Perkin Transactions 2 (1993) 799–805.
[45] E. Mullins, R. Oldland, Y.A. Liu, S. Wang, S.I. Sandler, C.-C. Chen, et al., Sigma-profile database for using COSMO-based thermodynamic methods, Industrial and Engineering Chemistry Research 45 (2006) 4389–4415.
[46] E. Mullins, Y.A. Liu, A. Ghaderi, S.D. Fast, Sigma profile database for predicting solid solubility in pure and mixed solvent mixtures for organic pharmacological compounds with COSMO-based thermodynamic methods, Industrial and Engineering Chemistry Research 47 (2008) 1707–1725.
[47] Y.T. Sato, T. Hamada, K. Kubo, A. Yamada, T. Kishida, O. Mazda, et al., Folding transition into a loosely collapsed state in plasmid DNA as revealed by single-molecule observation, FEBS Letters 579 (2005) 3095–3099.
[48] C. Schweitzer, J.C. Scaiano, Selective binding and local photophysics of the fluorescent cyanine dye PicoGreen in double-stranded and single-stranded DNA, Physical Chemistry Chemical Physics 5 (2003) 4911–4917.
[49] H. Nakanishi, K. Tsuchiya, T. Okubo, H. Sakai, M. Abe, Cationic surfactant changes the morphology of DNA molecules, Langmuir 23 (2007) 345–347.
[50] P. Misiak, B. Różycka-Roszak, E. Woźniak, R. Skrzela, K.A. Wilk, Aggregation study of omega-(alkyldimethylamonium)alkylaldonamide bromides, European Biophysics Journal with Biophysics Letters 40 (2011) 54.
[51] D. Matulis, I. Rouzina, V.A. Bloomfield, Thermodynamics of cationic lipid binding to DNA and DNA condensation: roles of electrostatics and hydrophobicity, Journal of the American Chemical Society 124 (2002) 7331–7342.
[52] S. Husale, W. Grange, M. Karle, S. Bürgi, M. Hegner, Interaction of cationic surfactants with DNA: a single-molecule study, Nucleic Acids Research 36 (2008) 1443–1449.
[53] J. Humpolíčková, L. Beranová, M. Stěpánek, A. Benda, K. Procházka, M. Hof, Fluorescence lifetime correlation spectroscopy reveals compaction mechanism of 10 and 49 kbp DNA and differences between polycation and cationic surfactant, The Journal of Physical Chemistry. B 112 (2008) 16823–16829.
[54] A.A. Zinchenko, V.G. Sergeyev, S. Murata, K. Yoshikawa, Controlling the intrachain segregation on a single DNA molecule, Journal of the American Chemical Society 125 (2003) 4414–4415.
[55] N. Miyazawa, T. Sakaue, K. Yoshikawa, R. Zana, Rings-on-a-string chain structure in DNA, The Journal of Chemical Physics 122 (2005) 44902.
[56] T. Parasassi, G. De Stasio, G. Ravagnan, R.M. Rusch, E. Gratton, Quantitation of lipid phases in phospholipid vesicles by the generalized polarization of Laurdan fluorescence, Biophysical Journal 60 (1991) 179–189.
[57] M. Suwalsky, C. Rodríguez, F. Villena, F. Aguilar, C.P. Sotomayor, The organochlorine pesticide lindane interacts with the human erythrocyte membrane, Pesticide Biochemistry and Physiology 62 (1998) 87–95.
[58] C.S. Pereira, P.H. Hünenberger, Interaction of the sugars trehalose, maltose and glucose with a phospholipid bilayer: a comparative molecular dynamics study, The Journal of Physical Chemistry. B 110 (2006) 15572–15581.
[59] K. Lohner, Effects of small organic molecules on phospholipid phase transitions, Chemistry and Physics of Lipids 57 (1991) 341–362.
[60] M.K. Jain, N.M. Wu, Effect of small molecules on the dipalmitoyl lecithin liposomal bilayer: III. Phase transition in lipid bilayer, The Journal of Membrane Biology 34 (1977) 157–201.